Running Title: The Drosophila muscle myosin relay-converter interface

The relay-converter interface influences hydrolysis of ATP by skeletal muscle myosin II

Marieke J. Bloemink[1,3], Girish C. Melkani[2], Sanford I. Bernstein[2†] and Michael A. Geeves[1†]

[1]School of Biosciences, University of Kent, Canterbury, United Kingdom, [2]Department of Biology, Molecular Biology Institute, and SDSU Heart Institute at San Diego State University, San Diego, CA, United States. [3]Present address: M.J. Bloemink, Biomolecular Research Group, School of Human and Life Sciences, Canterbury Christ Church University, Canterbury, United Kingdom.

[†] Corresponding Authors' Email: sbernstein@mail.sdsu.edu, m.a.geeves@kent.ac.uk

key words: muscle, myosin, kinetics, actin, fluorescence, homology models, sequence alignment, protein structure-function.

ABSTRACT

The interface between relay and converter domain of muscle myosin is critical for optimal myosin performance. Using *Drosophila melanogaster* indirect flight muscle S1 we performed a kinetic analysis of the effect of mutations in the converter and relay domain. Introduction of a mutation (R759E) in the converter domain inhibits the steady-state ATPase of myosin S1, whereas an additional mutation in the relay domain (N509K) is able to restore the ATPase towards wild-type values. The S1-R759E construct showed little effect on most steps of the actomyosin ATPase cycle. The exception was a 25-30% reduction in the rate constant of the hydrolysis step, the step coupled to the cross-bridge recovery stroke and involving a change in conformation at the relay/converter domain interface. Significantly the double mutant restored the hydrolysis step to values similar to the wild-type myosin. Modelling the relay/converter interface suggests a possible interaction between converter residue 759 and relay residue 509 in the actin-detached conformation, which is lost in R759E but is restored in N509K/R759E. This detailed kinetic analysis of *Drosophila* myosin carrying the R759E mutation shows that the interface between the relay loop and converter domain is important for fine-tuning myosin kinetics, in particular ATP-binding and hydrolysis.

The myosin family consists of at least 35 different classes (1), which display a wide range of activities, such as muscle contraction, phagocytosis, cell motility, tension maintenance and vesicle transport (2). Class II myosins are responsible for muscle contraction in higher eukaryotes and produce a variety of modes of muscle contraction. The type of myosin heavy chain isoform (MHC) predominantly expressed results in differing ATPase activity, unloaded shortening velocity, and contractile force (3). Although all myosins appear to undergo the same ATP driven cycle of interaction with actin, known as the cross-bridge cycle, it is still not well understood how they are each finely tuned to their different tasks (4).

Key events in the cross-bridge cycle are the actin.myosin power-stroke, which is thought to be closely coupled to the phosphate release step, and its reversal when detached from actin (the recovery stroke), which is coupled to the closure of switch 2 and the ATP cleavage step (5). Central to both power-stroke and recovery-stroke is the swing of the light chain binding domain or lever-arm which amplifies small movements in the nucleotide binding site to produce a movement of the end of the lever arm by up to 10 nm. The nucleotide site and the lever arm are linked through two structural elements: the converter domain and the relay loop-helix. Understanding the transmission of information through this pathway (nucleotide pocket -

relay helix - converter domain - lever arm) is a goal of current work.

Details of the interaction between the nucleotide site and the lever arm movement are best described for the recovery stroke, where crystal structures of myosin, complexed with analogues of ATP and ADP.Pi, have revealed high resolution structures of the pre- and post-recovery state conformations (6)(7) and allowed detailed molecular dynamic simulations of the transition between the two (8). In essence the presence of the γ-Pi in the nucleotide binding pocket allows the switch-2 element (SW2) to close and form a stable interaction with the Pi. SW-2 is at one end of the relay helix and the movement of SW-2 onto the Pi causes a twisting and bending of the relay helix such that the distal end of the relay helix goes through a large movement. The distal end of the relay element (relay loop) is in close contact with the converter (9) and as the relay moves, the converter moves with it and the lever arm amplifies the movement to a 5-10 nm translation of the myosin tail. The power stroke is to a first approximation considered a reversal of this recovery stroke while myosin is attached to actin and is coupled with loss of Pi from the nucleotide pocket. The lack of any high resolution structures during the power stroke means the molecular details of this event are less well defined. The contact between the relay helix and the converter is thus a central element in the efficient transmission of information between the nucleotide pocket and the lever arm, which we probe here.

Drosophila melanogaster is a classical model system for studying many eukaryotic proteins because of its well-developed tractable genetics. Muscle myosin II has been well studied in *Drosophila* because its function can be analysed at many different levels of organisation, allowing an integrative approach from the isolated myosin molecule through to the operating muscle in the adult fly (10)(11). Furthermore, all muscle myosin isoforms in *Drosophila* are expressed from a single gene (*Mhc*) using alternative splicing of a set of 6 exons, 4 of which are in the motor domain (12) (13). This allows expression of at least 21 different myosin isoforms and provides an exciting system to explore the role of the different exons in tuning the function of individual myosins for their biological role.

This work will focus on two alternatively spliced exons: exon 11 and exon 9. Exon 11 encodes for the converter region residues 724-764 of chicken fast skeletal myosin II or residues 721-761 of *Drosophila*, whereas exon 9 represents the 'relay helix-loop-helix domain' or 'relay domain' and corresponds to residues 472-528 of chicken myosin II (or residues 469-525 of *Drosophila*). The two variable regions encoded by exon 11 and 9 interact with each other, as shown in Figure 1A. Exchanging the converter region (exon 11) between the fast IFM (indirect flight muscle) and the slow EMB (embryonic) isoforms alters the mechanics and kinetics of the IFM and EMB fibres towards those of the donor isoform (14). Exchange of the relay domain (exon 9) between IFM and EMB does not alter the functional properties of the fast IFM myosin but does change the slow EMB myosin properties, *i.e*. reduced ATPase activity, increased actin affinity, eliminated actin motility, induced defects in myofibril assembly and rapid degeneration of muscle structure (15). Using motor domain or S1 fragments of chimeric constructs (IFI-9b and EMB-9a), transient kinetics studies also demonstrated reduced values for the rate constant of ATP-induced acto-myosin dissociation and ADP affinity for actin.S1 compared to both wild-type IFM and EMB S1 (16). Homology models indicated an important role for converter residue R759 in maintaining close contact (< 5Å) between the converter and the relay region (17), as is shown in Fig 1B.

As predicted from the modelling studies, the R759E mutation in the myosin of the indirect flight muscle of *Drosophila* resulted in major defects, including loss of flight, loss of myofibril stability and reduction of maximal power output (58%) (18). Studies with the isolated mutant myosin revealed reduced myosin ATPase activity and reduced actin velocity in *in vitro* motility assays (19). Following on from this work, it was reported that the double mutation R759E/N509K rescued many of the original R759E defects including flight ability, muscle ultrastructure, myosin ATPase and *in vitro* motility (17). These results confirm the important role of

R759 in maintaining the interaction between the converter and relay loop in IFI (indirect flight muscle isoform) myosin and its contribution to the high muscle power and optimal flight performance in *Drosophila*. The exact role of N509 in this process is currently not clear.

Here we follow up the recent work on the myosin R759E and R759E/N509K mutations. We have isolated the S1 motor domain from these mutant myosins and completed a biochemical kinetic study of the key events in the cross-bridge cycle. We find the effects of single and double mutations on the S1 ATPase activities are similar to full-length myosins but, surprisingly, we see little effect of the R759E mutation on the kinetics of the individual steps in the actin.S1 ATPase cycle. The exception is an inhibition of the ATP hydrolysis/recovery stroke by R759E, which is recovered in the R759E/N509K double mutation. The biological implications of this observation are discussed.

EXPERIMENTAL PROCEDURES.

Proteins: Monomeric G-actin was prepared from chicken skeletal muscle after several steps of polymerization–depolymerisation as recently described (17). Filamentous actin was prepared from G-actin and used for actin-stimulated ATPase activity (17) (20). Muscle myosin was isolated through multiple purification steps from microscopically dissected dorsolongitudinal indirect flight muscles of ~200 transgenic flies. Myosin subfragment 1 (S1), was prepared by chymotrypsin digestion as previously reported and the concentration of purified S1 was determined by spectrophotometry (16)(20).

*Steady state ATPase activity***:** Fresh S1 prepared after chymotrypsin digestion of myosin was used for steady state ATPase activity. S1 ATPase activities were determined using [γ-^{32}P]ATP as described (17)(20). Basal Ca^{2+} ATPase was determined as per full-length myosin and previously reported for S1 (15)(16). Both basal Mg^{2+} and actin-activated Mg^{2+}-ATPase were determined using Mg-ATPase buffer without KCl (10 mM imidazole, 0.1 mM $CaCl_2$, 1 mM $MgCl_2$, 1 mM [γ-^{32}P]ATP) as previously reported (20). Basal Mg^{2+}-ATPase activities obtained in the absence of actin were subtracted from all actin-activated data points. Actin-activated V_{max} and K_m values for actin were obtained by fitting all data points from several preparations of wild-type myosin S1 or mutant S1 with the Michaelis-Menten equation using SigmaPlot. Values were averaged to give mean ± S.D. Statistical differences of Ca^{2+} ATPase, Mg^{2+} ATPase, V_{max}, K_m and catalytic efficiency between wild-type, mutant and suppressor S1 were carried out using Student's *t* tests as previously described (20).

Flash photolysis system: Flash photolysis was used to measure the transient kinetics of the *Drosophila* myosin S1 mutants because of the small amounts of protein available (21)(22). By measuring changes in light scattering, the ATP-induced dissociation of the acto-S1 complex was followed after ATP release from caged-ATP using a laser pulse, whereas changes in fluorescence were used to measure the dissociation of nucleotide from S1 alone. For the fluorescence measurements S1 was incubated with a coumarin labeled ADP - analogue (3'-O-{N-[2-(7-diethylamino-coumarin-3-carboxamido)-ethyl]-carbamoyl ADP, abbreviated to deac-eda ADP) before displacement by ATP (23)(24). A low salt buffer was used for the light scattering experiments (pH 7.0: 30 mM KCl, 5 mM $MgCl_2$, 20 mM MOPS and 4 mM DTT) with 1 µM actin, 1-3 µM S1, 500 µM cATP (caged ATP), 10 mM DTT and either apyrase (2 units/ml), for ATP-induced dissociation of acto-S1 or ADP (various concentrations) and a glucose-hexokinase system (0.03 units/ml hexokinase, 1 mM glucose and 100 µM Ap_5A (P^1,P^5-di(adenosine 5')-pentaphosphate) for determination of K_{AD} as described previously (25). The light scattering traces were fitted with single exponentials to determine the k_{obs}. Hyperbolic plots of the k_{rel} (k_{obs}/k_0) vs. ADP concentration were fitted with an equation derived from Scheme 2 ($k_{obs} = K_1k_{+2}([ATP]/(1 + [ADP]/K_{AD}))$ to determine K_{AD} (see also 'analysis of transient kinetics' below).

Stopped-flow measurements: Measurements were performed with a High-Tech Scientific SF-61 DX2 stopped-flow system at 20 °C. Intrinsic tryptophan fluorescence was measured using a 295 nm excitation wavelength and observed through a WG320 filter (26). All stated concentrations of

reactants are those after mixing in the stopped-flow observation cell, unless otherwise specified. Stopped-flow data were analyzed using the Kinetic Studio software provided by TgK Scientific, as well as with Origin (Microcal).

Analysis of the transient kinetics data: Without actin present, the kinetics data of S1 with ATP (T) or ADP (D) were analyzed using the seven-step model described previously (27) The rate constants k_{+i} and k_{-i} are the forward and reverse rate constants and K_i (= k_{+i}/k_{-i}) represents the equilibrium constant of the *i*th step of the reaction (Scheme 1). In the presence of actin the stopped-flow kinetics data were analyzed based on Scheme 2. In order to determine the ADP-affinity in the presence of actin (K_{AD}) Equation 1 was used:

$$k_{obs} = K_1 k_{+2}([ATP]/(1 + [ADP]/K_{AD})) \quad (1)$$

where k_{obs} is the observed rate constant for the ATP-induced dissociation of acto-S1; $K_1 k_{+2}$ is the second-order rate constant for ATP binding to acto-S1; K_{AD} is the equilibrium dissociation constant for the binding of ADP to acto-S1. In order to determine the relative rate constant (k_{rel}) the equation $k_{rel} = k_{obs}/k_o$ was used (see Figure 4), where k_o is the measured rate constant k_{obs} when [ADP] = 0.

Homology Modelling: Three-dimensional homology models were generated for the *Drosophila* wild-type IFI myosin and converter mutant motor domains using the SWISS-MODEL (28) automatic comparative protein modelling server as described previously (16)(29). Briefly: the primary sequences of the *Drosophila* wild-type IFI and converter mutants were pairwise aligned with the sequence of four scallop myosin crystal structures as templates (ExPDB 1KK8, 1QVI, 1S5G and 1SR6 using the CLUSTALW alignment protocol and the alignments were submitted to the alignment interface of SWISS-MODEL (30) (31). The scallop myosin structures used as templates represent various conformational states of myosin during the cross-bridge cycle: the actin-detached state contains ADP-BeF_x (ExPDB: 1KK8), the pre-power stroke state contains ADP-VO_4 (ExPDB: 1QVI), a conformation that contains partially-bound ADP-SO_4 (ExPDB 1S5G) and the near-rigor state of myosin (ExPDB 1SR6) which does not have a nucleotide in the binding pocket. Although scallop templates represent multiple myosin states, they have an alanine at the equivalent position of N509 of *Drosophila* and may therefore not be the ideal templates to predict the sidechain conformation of N509. Chicken smooth muscle myosin has an aspartate at the equivalent position of N509. Therefore we also used chicken smooth structures as templates to build homology models for wild-type IFI, R759E and N509K/R759E (ExPDB: 1BR1, 1BR2, 1BR4 and 3J04) as smooth chicken myosin and *Drosophila* IFI share >50% of the myosin head domain sequence. The nucleotide binding pocket of smooth muscle myosin contains MgADP-AlF4 (1BR1, 1BR2) and MgADP-BeFx (1BR4) representing the pre-power stroke state (32). The 3J04 template is derived from phosphorylated smooth HMM chicken myosin in the presence of ATP (33). Overlay of crystal structures of myosin head domains of scallop (1SR6) and *Drosophila* embryonic myosin (4QBD) was done using the Visual Molecular Dynamics (VMD) software (34).

RESULTS

Steady state ATPase activity is reduced for R759E but (partially) restored for R759E/N509K.

Basal Ca^{2+}- and Mg^{2+}-ATPase activity of wild-type myosin S1 and the single and double mutants S1(R759E) and S1(R759E/N509K) were measured according to established procedures (20). As shown in Figure 2A and 2B the converter mutant R759E displayed a 2-fold reduction in basal Ca^{2+}-ATPase (2.26 ± 0.51 s^{-1}) and Mg^{2+}-ATPase (0.052 ± 0.016 s^{-1}) compared to wild-type IFI S1 (5.32 ± 0.62 s^{-1} and 0.092 ± 0.014 s^{-1} respectively). The double mutant (a potential suppressor) R759E/N509K was able to significantly restore both basal Ca^{2+}-ATPase (3.65 ± 0.69 s^{-1}) and Mg^{2+}-ATPase (0.073 ± 0.017 s^{-1}). As shown in Figure 2C the maximal actin-activated activity of R759E dropped to 30% of wild-type levels (V_{max} = 0.79 ± 0.23 s^{-1} and 2.54 ± 0.29 s^{-1}, respectively), whereas V_{max} of R759E/N509K showed 52% of wild-type activity (V_{max} = 1.31 ± 0.38 s^{-1}). Furthermore, the V_{max} of the

suppressor was significantly higher (1.31 ± 0.38 vs 0.79 ± 0.23 s^{-1}) than the V_{max} of the converter mutant R759E (Figure 2C). Unlike full-length myosin K_m (17), no significant change was found in K_m for actin between wild-type, R759E or R759E/N509K S1 (5.77 ± 0.83, 4.99 ± 1.23 and 3.58 ± 1.53 μM, respectively (Figure 2D). A ratio of V_{max}/K_m defined as catalytic efficiency (Figure 2E) (16)(17) was significantly lower in the R759E mutant (0.16 ± 0.03 $\mu M^{-1}s^{-1}$) compared to control and suppressor mutant N509K/R759E (0.44 ± 0.11 and 0.37 ± 0.12 $\mu M^{-1}s^{-1}$, respectively). In contrast, catalytic efficiencies of control and the suppressor mutant were statistically not different. Overall, the suppressor mutant N509K/R759E myosin S1 showed significant enhancement of basal Ca-ATPase, basal Mg-ATPase, and actin-stimulated Mg-ATPase activities compared with converter mutant (R759E) myosin S1, however, most of the ATPase data of the suppressor mutant remain significantly lower than wild-type control values.

ATP-induced dissociation and ADP-affinity of acto-S1 are similar to wild-type S1 for R759E and R759E/N509K.

The ATP-induced dissociation of the acto-S1 complex was measured as described previously using flash photolysis to liberate caged-ATP (21). Changes in light scattering were recorded and could be best described by a single exponential at each ATP concentration as shown in Figure 3A/B for R759E and the double mutant R759E/N509K). The slope of a graph of k_{obs} vs. ATP concentration defines the apparent second-order rate constant K_1k_{+2} for the dissociation of acto-S1 by ATP. The results for the two mutants together with the IFI wild-type S1 are depicted in Figure 3C and show that the K_1k_{+2} values are not significantly different for either of the two mutants compared to wild-type IFI (see Table 1). The ATP-induced dissociation of acto-S1 was also measured in the presence of increasing amounts of ADP in order to measure the affinity of ADP for actin.myosin, K_{AD}. Plotting k_{obs} versus ADP-concentration allows K_{AD} to be determined and the results are shown in Figure 3D. The measured values of K_{AD} for R759E or R759E/N509K are indistinguishable from the wild-type value (Table 1). Thus both ATP-induced dissociation and ADP-affinity of acto-S1are not affected for the two mutant myosin proteins.

ADP-release from S1-ADP (k_{-D}) is slower for the two converter mutants R759E and R759E/N509K compared to wild-type S1.

Using flash photolysis the rate constant of ADP dissociation from S1 in the absence of actin (k_{-D}) can be determined using the fluorescence of a coumarin labelled ADP (eda-deac ADP). Displacement of eda-deac ADP by ATP-binding to S1 results in a fluorescence change from which k_{-D} can be estimated. It was shown previously that this coumarin-labelled analogue has very similar kinetic properties to the unlabelled ADP (24). A single laser flash released 15-20 μM ATP from cATP (100 μM) and the fluorescence change resulting from eda-deac ADP release is well described by a single exponential function (data not shown). The observed rate constant for ADP release from S1 was slightly reduced (12-25 %) for the two converter mutants compared to wild-type S1 (Table 1).

Stopped-flow measurements shows altered ATP-binding and hydrolysis rate constants by S1 for both converter mutants.

Flash photolysis is usually the method of choice when measuring transient kinetics of *Drosophila* myosin S1 since this method requires much smaller quantities of protein (1 μg) compared to stopped-flow. Another reason is that stopped-flow measurements on *Drosophila* myosin were reported to yield relatively poor fluorescence signal changes when using pyrene-labeled actin whereas light scattering signals are very reproducible (22). However the laser flash with the caged ATP interferes with intrinsic fluorescence measurements precluding such measurements. The optical performance of stopped flow systems has improved recently and we re-examined the binding of ATP to *Drosophila* S1 monitoring intrinsic tryptophan fluorescence. Figure 4A shows the fluorescence change observed on rapidly mixing 10 μM ATP with 0.05 μM wild-type S1 at 20 °C (concentrations are post mixing). The transient increase in fluorescence is best described by a single exponential with an

observed rate constant k_{obs} = 54.7 s^{-1} and an amplitude of 3-4 %. Example traces of the fluorescence changes at high ATP are shown in Figure 4B and yield an observed rate constant k_{obs} = 260 s^{-1} for wild-type myosin S1. The amplitude of the transient was independent of the ATP concentration used. The dependence of k_{obs} on ATP concentration for wild-type S1 is shown in Figure 4C with a best fit to a hyperbola superimposed. The fit defines the second-order rate constant of ATP-binding K_1k_{+2} = 6.6 ± 0.6 x 10^6 $M^{-1}s^{-1}$, the maximum observed rate constant at saturating ATP concentrations (average value of k_{max} = 286 ±11 s^{-1}, see also table 1) and the ATP concentration required for the half maximal k_{obs} ($K_{0.5}$ = 85 µM).

Repeating this measurement with R759E-S1 and R759E/N509K S1 gave similar transients with amplitudes of 3-4 % (Figure 4A and 4B). The ATP dependence of the k_{obs} values is shown in Fig 4C and the average values of all fitted parameters are listed in Table 1. These show that the second order rate constant for ATP binding to single mutant R759E (2.7 ±0.9 x 10^6 $M^{-1}s^{-1}$) is significantly reduced to about half the value of the IFI-S1 (6.0±0.8 x 10^6 $M^{-1}s^{-1}$) while for the double mutant this value is significantly increased by about 1.5 fold (10 ±1 x 10^6 $M^{-1}s^{-1}$). Similarly the k_{max} value is reduced by 25 - 30 % for the single mutant while for the double mutant the value is again approximately 1.5 times increased but not significantly different to the wild-type value. In contrast, the value of $K_{0.5}$ for the double mutant (41 µM) is very similar to the wild-type value (53 µM) but the value for R759E (85 µM) is double the value of wild-type S1. This is in sharp contrast to the results for actin.S1 where the mutations have little effect on ATP or ADP binding. We must therefore contemplate carefully exactly what the different fluorescence signals are reporting, and this is considered in the Discussion

Interaction between converter residue R759 and relay residue N509 is regulated by SH1 residue F713.

Homology models were built of wild-type IFI and the two mutants R759E and R759E/N509K. The available scallop myosin-II motor domain crystal structures were initially used as templates, as these represent many different states in the myosin cross-bridge cycle (16). Recently the first crystal structure of myosin S1 from *Drosophila* (embryonic isoform) has become available (PDB: 4QBD). This structure is very similar to the corresponding scallop crystal structure (1SR6), as shown in Figure 5A, with an overall backbone rmsd < 1.8 Å. The scallop structures have an arginine residue (R754) in the converter domain at the equivalent position as *Drosophila* R759, but in the relay loop area scallop has an alanine instead of asparagine at the equivalent position of *Drosophila* N509 (Figure 5B). The homology models show that converter residue R759 interacts with residues located in the relay loop, in the converter and in the SH1 helix and that, not surprisingly, these interactions depend on the conformational state of the myosin head.

In wild-type myosin S1 (IFI-S1) residue R759 forms a salt bridge with D756, another converter residue. This salt bridge is preserved in all homology models of IFI-S1 (Figure 1B) and also present in the *Drosophila* embryonic myosin crystal structure. Residue F713, located in the SH1 helix, interacts with R759 and this interaction is seen in all models of the myosin states, except the actin-detached state (Figure 6). The homology models suggest the presence of a π-cation bond between SH1-helix residue F713 and converter residue R759. The presence of a π-cation bond, together with a salt-bridge towards D756, holds the R759 side chain oriented towards the converter domain and prevents it from making contacts with the relay loop in the pre-power-stroke and near-rigor states. In the actin-detached state (1KK8 template) F713 has moved away from R759, as the SH1 helix becomes disordered, and the π-cation bond is lost. R759 now forms strong H-bonds with the backbone C=O of residue N509 in the relay loop while maintaining a salt bridge with converter residue D756 (Figure 7 and also Figure 1). The two mutants also show H-bonds between the side chain of residue 759 (E759 for both mutants) and the backbone NH of residue 509 (N509 or K509) in the actin-detached state. However, the mutants are missing the salt bridge seen for wild-type IFI from residue 759 towards D756 (Figure 7). Thus the homology models (based on scallop myosin-II templates) suggest that the two mutants have fewer interactions between the

converter and relay domain compared to wild-type IFI.

Interaction between converter residue 759 and relay residue 509 is disrupted in R759E and restored in N509K/R759E.

Fewer interactions between the converter and relay loop, as discussed above, can account for the loss of activity seen for R759E but do not provide an explanation for the restored activity in R759E/N509K. Scallop templates, although very useful because of the multiple myosin states available, have an alanine at the equivalent position of N509 of *Drosophila* (Figure 5B) and may therefore not be the best templates to represent the side chain conformation of N509. Chicken smooth muscle myosin has a glutamate (E511) at the equivalent position of N509 (Figure 5B) and could potentially provide a better template to build a homology model that represents the structure of the N509 side chain more accurately. The chicken smooth crystal structures all show a salt-bridge between relay residue E511 and R768 (R759 equivalent). Using chicken smooth muscle myosin as a template we built homology models for wild-type IFI, R759E and N509K/R759E and the results are summarised in Figure 8. For wild-type IFI the homology model (using the smooth myosin 3J07 structure as template) predicts a direct interaction via hydrogen bonds between the side-chains of R759 and N509 within a distance of 2.9 – 4.5 Å (Figure 8A), which is disrupted when R759 is replaced by E759 (Figure 8B). For N509K/R759E this interaction is restored, as the homology model predicts the side-chains of E759 and K509 are within < 3.0 Å and can form a salt bridge (Figure 8C). These observations correlate very well with the loss of activity seen for R759E and the restored activity for N509K/R759E.

DISCUSSION

The relay-converter interface has been implicated in the communication pathway between the nucleotide binding site and the lever arm movement (8) and altering this interface can severely disrupt the communication pathway. The interface between the converter and relay helix is believed to be maintained throughout the myosin cross-bridge cycle (9) and its alteration can significantly disrupt the performance of the indirect flight muscle (18) and impair flight ability (19). Additionally, our previous work showed that introducing a R759E mutation in the converter region of full-length myosin reduces ATPase activity and *in vitro* motility and also disrupts flight ability and power generation in *Drosophila* IFM (19). Interestingly, the defects reported for R759E can be suppressed by a second mutation (N509K) in the relay domain. This N509K mutation can restore ATPase activity, *in vitro* motility and can also rescue the ability of *Drosophila* carrying the R759E to fly (17). Our steady-state kinetics analysis of isolated S1 fragment verified the effects seen in ATPase activity for full-length myosin. Our transient kinetics analysis sought to identify which step(s) in the cross-bridge cycle are affected by the mutation and the suppressor. Of significance, our data show that the ATP hydrolysis step is strongly affected. This step is known to be coupled to the recovery-stroke which involves the movement of the relay helix and the converter domain (8).

Our transient kinetics data show surprisingly little change in any of the kinetic parameters measured, except those determined in the absence of actin, i.e., ATP binding to S1 and its hydrolysis. ATP binding (K_1k_{+2}) to the single mutant R759E is about half the value found for wild-type S1, while for the double mutant the value is increased by about 1.5 fold of the wild-type value. Similarly the k_{max} value is reduced by 25 % for the R759E mutant while for the double mutant the value is higher than found for wild-type S1, although this difference is not statistically significant. The tryptophan changes observed when ATP interacts with myosin S1 can have two components: one from the ATP binding step, (signalled from tryptophan(s) near the nucleotide binding pocket) and another one from the recovery stroke/ATP hydrolysis step signalled by the highly conserved tryptophan at the end of the relay helix (see Figure 6) that senses the converter movement (35). *Drosophila* myosin has the conserved relay loop tryptophan W510 next to the mutated N509, and is therefore expected to give a signal change on the recovery stroke/ hydrolysis. In contrast ADP binding gives

little change in fluorescence, suggesting little effect on nucleotide binding and that the major contribution of the fluorescence change does originate in the converter domain movement. The standard model for the ATP binding and hydrolysis by myosin is then:

$$M + T \overset{1}{\longleftrightarrow} MT \xrightarrow{2} M'T \overset{3}{\longleftrightarrow} M{\bullet}D{\bullet}P{\bullet}Pi$$

If the fluorescence change occurs only in step 3 (ATP hydrolysis), then at low [ATP] such that $k_{+3} + k_{-3} >> K_1k_{+2}$[ATP], k_{obs} has a linear dependence upon ATP concentration i.e., $k_{obs} = K_1k_{+2}$[ATP]. At high [ATP] such that $k_{+3} + k_{-3} << K_1k_{+2}$ [ATP], k_{obs} is independent of [ATP] and $k_{obs} = k_{+3} + k_{-3}$. Over the full range of ATP concentrations, the dependence of k_{obs} on [ATP] approximates to a hyperbola as shown in Fig 4C. A test for such a model is the observed value of the [ATP] required for half maximal value of k_{obs} ($K_{0.5}$ in Table 1). $K_{0.5}$ is the ATP concentration at which the $k_{+3} + k_{-3} = K_1k_{+2}$[ATP]. Inspection of the values listed in Table 1 shows this to be true for all three S1 constructs used. Thus we can assign k_{max} to $k_{+3} + k_{-3}$ and the apparent second order rate constant to $K_1k_{+2.}$ The value of $K_{0.5}$ has no specific meaning in the mechanism.

The implications from this analysis are that the mutations are affecting how ATP binds to S1 (K_1k_{+2}) and also the apparent rate constant of the ATP hydrolysis step $k_{+3} + k_{-3}$. The change in K_1k_{+2} could be due to a change in K_1 or k_{+2} or both. Step 1 is the initial binding of ATP into the nucleotide pocket and step 2 is the induced change in S1 structure associated with switch 1 closure. Any mutation can alter the stability of the apo protein and potentially disturb the conformation of the binding pocket. Since we do not see any inhibition of ATP binding to actoS1 it suggests that actin stabilises the "native like" structure of the myosin and specifically the nucleotide binding pocket.

Step 3 combines the closure of switch 2, the recovery or re-priming stroke of the myosin head and the ATP hydrolysis step. The assumption is usually made that these steps are present for all myosins and we will make that assumption here. In this model the closing of the switch 2 loop onto the gamma Pi of ATP is required to position the catalytic residues to allow hydrolysis of ATP. At the same time closure of switch 2 twists the relay helix and results in a change in the position of the converter domain and thereby the lever arm goes through its recovery stroke. Note that R759 on the converter and N509 on the relay helix are part of the structural elements involved in the recovery stroke (36)(7) and mutations here may therefore be expected to influence the hydrolysis step and recovery stroke. The energetics of the recovery stroke and ATP hydrolysis have been well defined for one myosin, the *Dictyostelium* myosin II (8)(37). In *Dictyostelium* myosin II the equilibrium constants for the recovery stroke and the subsequent hydrolysis step are both quite small (values 0.1-10) and the overall equilibrium constants for the combined step for many muscle myosin IIs are also small, i.e., <10. Thus the system is balanced energetically and hence susceptible to perturbation by small structural changes anywhere along the pathway from the nucleotide pocket to the lever arm and many such perturbations have been reported.

Mutations in myosin are instructive in defining domains that are critical for ATPase activity and coupling of the nucleotide pocket to the lever arm. Introduction of point mutations at the base of the myosin lever arm (Lys84Met and Arg704Glu) changes the equilibrium constant of the recovery stroke and also alters the ATP-hydrolysis rate constant (37) Truncation of the myosin head changed the ATP-hydrolysis rate constant in *Dictyostelium* myosin II. Truncations at residue 761, 781, and 864 give myosin fragments with zero (M761), one (M781) or two (M864) light chain binding sites and the shorter M761 fragment displayed the fastest hydrolysis rate constant (160 s^{-1}) compared to the longer fragments M781 (37 s^{-1}) and M864 (24 s^{-1}) (38). Apart from changes in the hydrolysis rates, the myosins were largely similar to each other. Mutation of two hydrophobic contacts with the converter domain, I499 in the relay loop and F692 in the SH2 region, resulted in uncoupling of the converter rotation and ATP-hydrolysis and a complete loss of *in vivo* and *in vitro* motility (39). In other myosin classes the equilibrium constant for the recovery stroke and ATP-hydrolysis may be very different compared to myosin-II. A recently reported crystal structure of myosin-Ib, a very tension-sensitive myosin,

revealed a 10-residue stretch of N-terminal amino acids that stabilizes the post-power stroke conformation by making hydrophobic contacts with both the motor and the lever arm helix domain (40, 41). Such contacts have been proposed to play a role in the tension sensing mechanism of this myosin.

Variations in the converter domain have been found to influence the contractile properties of myosin in muscles. Exchanging the converter domain between the fast IFI and slow EMB isoforms of *Drosophila* myosin resulted in a shift in contractile properties towards the donor isoform (14). However, this converter swap did not completely exchange the contractile properties between IFI and EMB, suggesting other variable regions in the myosin head contribute as well. Exchange of exon 9 between the IFI and EMB isoforms also significantly affected the mechanical properties of the muscle fibres but again did not result in a complete conversion from EMB to IFI and vice versa (42). Three embryonic myosin isoforms, expressing alternative converter and/or relay domains, were found to have different ATPase activity, *in vitro* motility and muscle ultrastructure and thus suggested that different forms of relays and converters are used to fine-tune myosin properties (14).

Biochemical studies only assess unloaded transitions in the cross bridge cycle. Under loaded conditions the detached states are the same but the attached part of the cycle may be very different. The evidence from muscle fibre studies is that the converter/relay loop is important for mechanical coupling. Detailed mechanics measurements, using IFM fibres from *Drosophila*, found a significant reduction in muscle power for fibres containing the R759E mutation compared to wild-type fibres (18). The reduced power of R759E IFM fibres was attributed to a decrease in work production due to slower work production, the 2πb component of sinusoidal analysis. No changes were found for the work-absorbing steps (2πc component of sinusoidal analysis), which includes myosin detachment from actin. Our kinetics data show no significant change in steps controlling myosin detachment from actin, ADP-affinity and ATP-induced dissociation, consistent with no change in the 2πc component from the mechanics study (18). Our experiments cannot assess the work producing steps of the cycle (2πb), however the recovery step and hydrolysis step do involve the reversal of the structural changes associated with the power stroke. Notably the hydrolysis step for R759E was reduced 70% compared to wild-type IFI, while the mechanics study reported a reduction of 68% of the 2πb component for R759E compared to wild-type myosin.

The suppressor R759E/N509K is able to substantially restore *in vitro* motility and myofibril assembly and also rescue flight ability (17) and our results show a significant increase in ATPase activity and ATP-binding and hydrolysis compared to R759E, although not to wild-type levels. These observations suggest that an interaction between residue 759 and 509 is necessary for optimal myosin activity. The ability of the double mutation to restore near normal function to the myosin might be interpreted to suggest a salt bridge between the two residues. Our molecular models, using chicken smooth muscle myosin as a template, do predict the presence of a salt bridge between the side-chains of residues 759 and 509 in the double mutant. It cannot be excluded that this salt bridge is also formed during other stages of the myosin cross-bridge cycle that are not yet represented in the scallop crystal structures as suggested previously (17).

In conclusion, we find that the interface between relay and converter domain of muscle myosin is critical for optimal myosin performance. Introduction of a mutation (R759E) in the converter domain impairs the steady-state and transient kinetic properties of myosin R759E S1 compared to wild-type S1. Our biochemical approach allows us to identify ATP-binding and ATP hydrolysis as the steps that are significantly affected by the R759E mutation, and agree with earlier mechanical data for R759E. Introducing a second mutation on the other side of the converter-relay interface in the relay domain (N509K) results in enhanced steady-state and transient kinetics, with a significant increase in ATP-binding and hydrolysis for R759E/N509K. Molecular modelling suggests that formation of a salt bridge between these two residues serves as the basis for the observed rescue.

Acknowledgements:

This work was supported by NIH grant GM32443 (to SIB) and Wellcome Trust Grant 085309 (to MAG). We thank Martin Webb (National Institute for Medical Research, Mill Hill, London, UK) for the coumarin ATP/ADP used in this work and Anju Melkani (SDSU) and Sam Lynn (University of Kent) for excellent technical support.

Conflict of interest:

The authors declare that they have no conflicts of interest with the contents of this article.

Author contributions:

MB performed flash photolysis, stopped-flow and homology modelling work. GM did the S1 protein purification and ATPase assays. SB and MG designed the research. MB, GM, SB and MG contributed to data analysis and writing of the manuscript. All authors approved of the final manuscript before submission.

REFERENCES

1. Odronitz, F., and Kollmar, M. (2007) Drawing the tree of eukaryotic life based on the analysis of 2,269 manually annotated myosins from 328 species. *Genome Biol*. **8**, R196

2. O'Connell, C. B., Tyska, M. J., and Mooseker, M. S. (2007) Myosin at work: motor adaptations for a variety of cellular functions. *Biochim. Biophys. Acta (BBA)-Molecular Cell Res.* **1773**, 615–630

3. Reggiani, C., Bottinelli, R., and Stienen, G. J. M. (2000) Sarcomeric Myosin Isoforms: Fine Tuning of a Molecular Motor. *Physiology*. **15**, 26–33

4. Bloemink, M. J., and Geeves, M. A. (2011) Shaking the myosin family tree: biochemical kinetics defines four types of myosin motor. *Semin. Cell Dev. Biol.* **22**, 961–7

5. Geeves, M. A., Fedorov, R., and Manstein, D. J. (2005) Molecular mechanism of actomyosin-based motility. *Cell. Mol. Life Sci. C.* **62**, 1462–1477

6. Houdusse, A, Szent-Gyorgyi, a G., and Cohen, C. (2000) Three conformational states of scallop myosin S1. *Proc. Natl. Acad. Sci. U. S. A.* **97**, 11238–43

7. Holmes, K. C., Schröder, R. R., Sweeney, H. L., and Houdusse, A. (2004) The structure of the rigor complex and its implications for the power stroke. *Philos. Trans. R. Soc. Lond. B. Biol. Sci.* **359**, 1819–28

8. Koppole, S., Smith, J. C., and Fischer, S. (2007) The structural coupling between ATPase activation and recovery stroke in the myosin II motor. *Structure*. **15**, 825–37

9. Shih, W. M., and Spudich, J. A. (2001) The myosin relay helix to converter interface remains intact throughout the actomyosin ATPase cycle. *J. Biol. Chem.* **276**, 19491–4

10. Swank, D. M., Wells, L., Kronert, W. A., Morrill, G. E., and Bernstein, S. I. (2000) Determining structure/function relationships for sarcomeric myosin heavy chain by genetic and transgenic manipulation of Drosophila. *Microsc. Res. Tech.* **50**, 430–442

11. Vigoreaux, J. O. (2001) Genetics of the Drosophila flight muscle myofibril : a window into the biology of complex systems. *BioEssays*. **23**, 1047–1063

12. George, E. L., Ober, M. B., and Emerson, C. P. (1989) Functional domains of the Drosophila melanogaster muscle myosin heavy-chain gene are encoded by alternatively spliced exons. *Mol. Cell. Biol.* **9**, 2957–74

13. Bernstein, S. I., and Milligan, R. A. (1997) Fine tuning a molecular motor: the location of alternative domains in the Drosophila myosin head. *J. Mol. Biol.* **271**, 1–6

14. Swank, D. D. M., Knowles, A. F. A., Suggs, J. A. J., Sarsoza, F., Lee, A., Maughan, D. W., and Bernstein, S. I. (2002) The myosin converter domain modulates muscle performance. *Nat. Cell Biol.* **4**, 312–316

15. Kronert, W. A., Dambacher, C. M., Knowles, A. F., Swank, D. M., and Bernstein, S. I. (2008) Alternative relay domains of Drosophila melanogaster myosin differentially affect ATPase activity, in vitro motility, myofibril structure and muscle function. *J. Mol. Biol.* **379**, 443–56

16. Bloemink, M. J., Dambacher, C. M., Knowles, A. F., Melkani, G. C., Geeves, M. A., and Bernstein, S. I. (2009) Alternative exon 9-encoded relay domains affect more than one communication pathway in the Drosophila myosin head. *J. Mol. Biol.* **389**, 707–21

17. Kronert, W. A., Melkani, G. C., Melkani, A., and Bernstein, S. I. (2014) Mapping interactions between myosin relay and converter domains that power muscle function. *J. Biol. Chem.* **289**, 12779–90

18. Ramanath, S., Wang, Q., Bernstein, S. I., and Swank, D. M. (2011) Disrupting the myosin converter-relay interface impairs Drosophila indirect flight muscle performance. *Biophys. J.* **101**, 1114–22

19. Kronert, W. A., Melkani, G. C., Melkani, A., and Bernstein, S. I. (2010) Mutating the converter-relay interface of Drosophila myosin perturbs ATPase activity, actin motility, myofibril stability and flight ability. *J. Mol. Biol.* **398**, 625–32

20. Bloemink, M. J., Melkani, G. C., Dambacher, C. M., Bernstein, S. I., and Geeves, M. A. (2011) Two Drosophila myosin transducer mutants with distinct cardiomyopathies have divergent ADP and actin affinities. *J. Biol. Chem.* **286**, 28435–43

21. Weiss, S., Chizhov, I., and Geeves, M. A. (2000) A flash photolysis fluorescence/light scattering apparatus for use with sub microgram quantities of muscle proteins. *J. Muscle Res. Cell Motil.* **21**, 423–32

22. Silva, R., Sparrow, J. C., and Geeves, M. A. (2003) Isolation and kinetic characterisation of myosin and myosin S1 from the Drosophila indirect flight muscles. *J. Muscle Res. Cell Motil.* **24**, 489–98

23. Webb, M. R., and Corrie, J. E. T. (2001) Fluorescent Coumarin-Labeled Nucleotides to Measure ADP Release from Actomyosin. *J. Muscle Res. Cell Motil.* **81**, 1562–1569

24. Clark, R. J., Nyitrai, M., Webb, M. R., and Geeves, M. A. (2003) Probing nucleotide dissociation from myosin in vitro using microgram quantities of myosin. *J. Muscle Res. Cell Motil.* **24**, 315–21

25. Miller, B. M., Nyitrai, M., Bernstein, S. I., and Geeves, M. A. (2003) Kinetic analysis of Drosophila muscle myosin isoforms suggests a novel mode of mechanochemical coupling. *J. Biol. Chem.* **278**, 50293–300

26. Bloemink, M. J., Adamek, N., Reggiani, C., and Geeves, M. A. (2007) Kinetic analysis of the slow skeletal myosin MHC-1 isoform from bovine masseter muscle. *J. Mol. Biol.* **373**, 1184–97

27. Bagshaw, C. R., Eccleston, J. F., Eckstein, F., Goody, R. S., Gutfreund, H., and Trentham, D. R. (1974) The magnesium ion-dependent adenosine triphosphatase of myosin. Two-step processes of adenosine triphosphate association and adenosine diphosphate dissociation. *Biochem. J.* **141**, 351–364

28. Schwede, T. (2003) SWISS-MODEL: an automated protein homology-modeling server. *Nucleic Acids Res.* **31**, 3381–3385

29. Schwede, T., Kopp, J., Guex, N., and Peitsch, M. C. (2003) SWISS-MODEL: an automated protein homology-modeling server. *Nucleic Acids Res.* **31**, 3381–3385

30. Arnold, K., Bordoli, L., Kopp, J., and Schwede, T. (2006) The SWISS-MODEL workspace: a web-based environment for protein structure homology modelling. *Bioinformatics*. **22**, 195–201

31. Biasini, M., Bienert, S., Waterhouse, A., Arnold, K., Studer, G., Schmidt, T., Kiefer, F., Cassarino, T. G., Bertoni, M., Bordoli, L., and Schwede, T. (2014) SWISS-MODEL: modelling protein tertiary and quaternary structure using evolutionary information. *Nucleic Acids Res.* 10.1093/nar/gku340

32. Dominguez, R., Freyzon, Y., Trybus, K. M., and Cohen, C. (1998) Crystal structure of a vertebrate smooth muscle myosin motor domain and its complex with the essential light chain: visualization of the pre-power stroke state. *Cell*. **94**, 559–71

33. Baumann, B. A. J., Taylor, D. W., Huang, Z., Tama, F., Fagnant, P. M., Trybus, K. M., and Taylor, K. A. (2012) Phosphorylated smooth muscle heavy meromyosin shows an open conformation linked to activation. *J. Mol. Biol.* **415**, 274–287

34. Humphrey, W., Dalke, A., and Schulten, K. (1996) VMD: visual molecular dynamics. *J. Mol. Graph.* **14**, 33–38

35. Málnási-Csizmadia, A., Woolley, R. J., and Bagshaw, C. R. (2000) Resolution of conformational states of Dictyostelium myosin II motor domain using tryptophan (W501) mutants: implications for the open-closed transition identified by crystallography. *Biochemistry*. **39**, 16135–16146

36. Houdusse, A., Szent-Györgyi, A. G., and Cohen, C. (2000) Three conformational states of scallop myosin S1. *Proc. Natl. Acad. Sci.* **97**, 11238–11243

37. Málnási-Csizmadia, A., Tóth, J., Pearson, D. S., Hetényi, C., Nyitray, L., Geeves, M. A., Bagshaw, C. R., and Kovács, M. (2007) Selective perturbation of the myosin recovery stroke by point mutations at the base of the lever arm affects ATP hydrolysis and phosphate release. *J. Biol. Chem.* **282**, 17658–64

38. Kurzawa, S. E., Manstein, D. J., and Geeves, M. A. (1997) Dictyostelium discoideum Myosin II: Characterization of Functional Myosin Motor Fragments. *Biochemistry*. **36**, 317–323

39. Sasaki, N., Ohkura, R., and Sutoh, K. (2003) Dictyostelium myosin II mutations that uncouple the converter swing and ATP hydrolysis cycle. *Biochemistry*. **42**, 90–5

40. Shuman, H., Greenberg, M. J., Zwolak, A., Lin, T., Sindelar, C. V, Dominguez, R., and Ostap, E. M. (2014) A vertebrate myosin-I structure reveals unique insights into myosin mechanochemical tuning. *Proc. Natl. Acad. Sci.* . **111** , 2116–2121

41. Greenberg, M. J., Lin, T., Shuman, H., and Ostap, E. M. (2015) Mechanochemical tuning of myosin-I by the N-terminal region. *Proc. Natl. Acad. Sci.* . 10.1073/pnas.1506633112

42. Yang, C., Ramanath, S., Kronert, W. A., Bernstein, S. I., Maughan, D. W., and Swank, D. M. (2008) Alternative versions of the myosin relay domain differentially respond to load to influence Drosophila muscle kinetics. *Biophys. J.* **95**, 5228–37

FIGURE LEGENDS:

Table 1: Transient kinetic parameters measured for *Drosophila* myosin S1 mutants R759E and R759E/N509K compared to wild-type IFI S1. Values are mean ± S.D. based on a minimum of 3 preparations.

Figure 1: Overview of myosin S1 with relay area (yellow) and converter domain (red) indicated. (A) The residues 509 (relay loop) and 759 (converter) are shown as space-filling models. The nucleotide is also shown at the opposite end of the relay helix. (B) Close-up of the interface between the relay loop and converter domain with converter residue R759 interacting with variable relay loop residue N509 and converter residue D756. Homology model of the *Drosophila* IFI myosin isoform was built using the coordinates of PDB 1KK8 (actin-detached post power-stroke state) as a template.

Figure 2: Steady State ATPase activity of wild-type control, single mutant R759E and double mutant R759E/N509K *Drosophila* myosin. Basal Ca-ATPase activity (A), basal Mg-ATPase activity (B), actin-stimulated Mg-ATPase activity V_{max} (C), actin affinity relative to Mg-ATPase (K_m) (D) and catalytic efficiency (E) were determined as described in the Materials and Methods. Notations above histograms indicate the level of statistically significant differences (*=p<0.05, **=p<0.01, ***=p<0.001, ns= not statistically significant). Significant differences were assumed for p<0.05.

Figure 3: Summary of transient kinetics measurements of converter mutant and suppressor. (A/B) Example of light scattering traces measured for R759E *(*panel A) and R759E/N509K (panel B) using flash photolysis and fitted to single exponentials, from which the rate constant k_{obs} is determined. (C) k_{obs} as a function of [ATP] yields the acto-myosin dissociation constant K_1k_{+2} which is not significantly different for R759E and R759E/N509K compared to wild-type. (D) ATP-induced dissociation of acto-S1 with increasing [ADP] shows similar ADP-affinity (K_{AD}) for R759E and R759E/N509K compared to IFI-wt.

Figure 4: ATP binding to Drosophila S1.

Intrinsic fluorescence transients observed for ATP-binding to wild-type myosin S1 and converter mutants R759E and R759E/N509K S1 using stopped-flow. 50 nM S1 is rapidly mixed with A) 10 µM ATP or B) 320 µM ATP (IFI-wt and R759E) or 160 µM ATP (R759E/N509K). Note that the amplitudes are small (2-3%) and evaluation of k_{obs} values above 200 s^{-1} becomes unreliable. (C) Summary of stopped-flow data: k_{obs} as a function of [ATP] yields k_{max} = 223 s^{-1} (R759E), 322 s^{-1} (R759E/N509K) and 286 s^{-1} (IFI-wt) for a single data set measured for wild-type S1, R759E and R759E/N509K.

Figure 5: The myosin head domains of scallop and *Drosophila* are very similar. (A) Overlay of crystal structures of myosin head domains of scallop (1RS6) and *Drosophila* embryonic myosin (4QBD). The colouring represents the rmsd values between the two structures with similar structural elements shown in blue and deviating structural elements (large rmsd values) shown in red. The backbone of the two structures overlay very well with an average rmsd < 1.8 Å (shown in blue). Flexible loops that diverge somewhat are shown in red. (B) Alignments for *Drosophila* (IFI and EMB), scallop and chicken smooth myosin. The conserved residues R759 and F713 in the converter area (bottom) are highlighted in yellow. Note that in regard to the variable residues surrounding the conserved tryptophan (yellow box in the relay loop) the N509 residue (*Drosophila* IFI) is replaced by alanine (scallop) and glutamate (chicken smooth).

Figure 6: Interaction between converter residue R759 and SH1 helix residue F713. Top panels: Homology models of IFI-wt indicate a strong interaction between R759 and F713 in near-rigor (yellow) and pre-power-stroke state (red) whereas in the post-power-stroke state (blue) this interaction is not seen, as SH1 has become disordered. Bottom panel: Overlay of the models for IFI-wt myosin

showing the SH1/SH2 and converter area for different myosin conformations. The SH2 area overlays very well but structures start to divert in SH1 area. Residue R759 is indicated for each conformation, together with F713. Homology models of the *Drosophila* IFI myosin isoform were built using the coordinates of scallop myosin PDB 1QVI (pre-power stroke state), PDB 1SR6 (near-rigor state) and PDB 1KK8 (actin-detached post power stroke state) as a templates.

Figure 7: Details of the relay-converter interaction. (A) R759 of wild-type IFI in the pre-power stroke state cannot make contacts with relay loop residues and makes contacts with converter residues (P755/D756) and SH1 residue F713. (B) In the post-power stroke state (actin-detached) R759 contacts relay residue N509 and W510, in addition to converter residues (P755/D756). F713 has moved away after SH1 helix structure is lost. (C) The R759E mutant residue is able to contact relay loop residue N509 as well in the post-power stroke/actin-detached state. However, additional contacts with converter residues P755/D756 are missing. Homology models were built using scallop myosin PDB 1QVI (pre-power stroke) and PDB 1KK8 (actin-detached, post power stroke state) as a templates.

Figure 8: Side-chain interactions between converter residue 759 and relay loop residue 509 for wild-type IFI (A), R759E (B) and N509K/R759E (C) (A) Close-up of the interface between the relay loop and converter domain with converter residue R759 interacting with the side-chain of residue N509 , via H-bonds, and converter residue E755 via a salt-bridge. (B) Close-up of the interface between the relay loop and converter domain of R759E S1 mutant: converter residue E759 only forms H-bonds with backbone NH of N509. (C) Close-up of the interface between the relay loop and converter domain of N509K/R759E S1 mutant: Interaction between the sidechains of residue 759 and 509 is restored as the side chains are close enough to form a salt-bridge. (homology model built using the coordinates of chicken smooth muscle myosin in the pre-power stroke state (PDB 3J04) as a template).

Scheme I: The interaction of S1 with ATP and ADP. S1, ATP and ADP are represented as M, T and D, respectively. * indicates the different levels of tryptophan fluorescence and represents different conformational states of the myosin.

Scheme 2: The interaction of S1 with actin, ATP and ADP. Myosin, actin, ATP and ADP are represented as M, A, T and D, respectively. Dashed (-) interactions represent a weakly bound complex and dotted (·) interactions represent strongly bound states. Cross-bridge detachment from the rigor state (A·M) involves the complex binding ATP, governed by the association constant, K'_1, followed by the rate-limiting isomerization, k'_{+2}, after which actin-myosin affinity becomes weak and the complex separates rapidly.

Table 1: Transient kinetic parameters measured for *Drosophila* myosin S1 mutants R759E and R759E/N509K compared to wild-type IFI S1. Values are mean ± S.D. based on a minimum of 3 preparations.

	wild-type S1	R759E S1	R759E/N509K S1
acto-S1 dissociation[a] $K'_1k'_{+2}$ ($\mu M^{-1}s^{-1}$)	0.70 ± 0.10	0.72 ± 0.09	0.70 ± 0.05
ADP-affinity of acto-S1[a] K_{AD} (μM)	406 ± 25[c]	428 ± 20	421 ± 41
ADP-release from S1[a] k_{-D} (s^{-1})	8.0 ± 0.5	7.0 ± 0.4[d]	6.0 ± 0.3[d]
ATP-binding to S1[b] K_1k_{+2} ($\mu M^{-1}s^{-1}$)	6.0±0.8	2.7 ±0.9[e]	10 ± 1[e]
$k_{+3}+ k_{-3}$ (s^{-1})	308 ± 35	223 ± 28[e]	404 ± 111
$1/K_{0.5}$ (μM)	53±12	85±30	41±8

[a] measured for this study using flash photolysis. [b] measured for this study using stopped-flow. [c] K_{AD} value is from (25) [d] Significantly different from IFI as determined by the student's t-test ($p<0.005$). [e] Significantly different from wild-type S1 as determined by the student's t-test ($p<0.05$).

Figure 1:

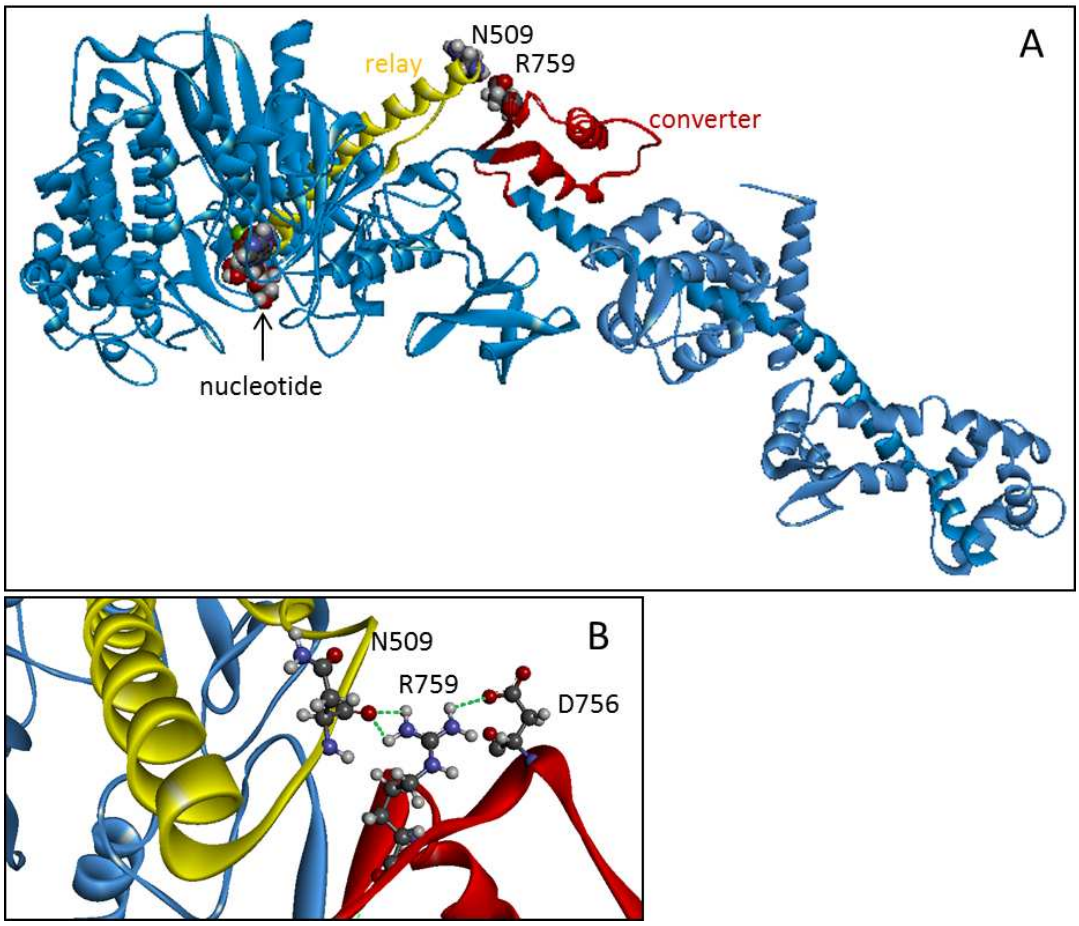

Figure 2:

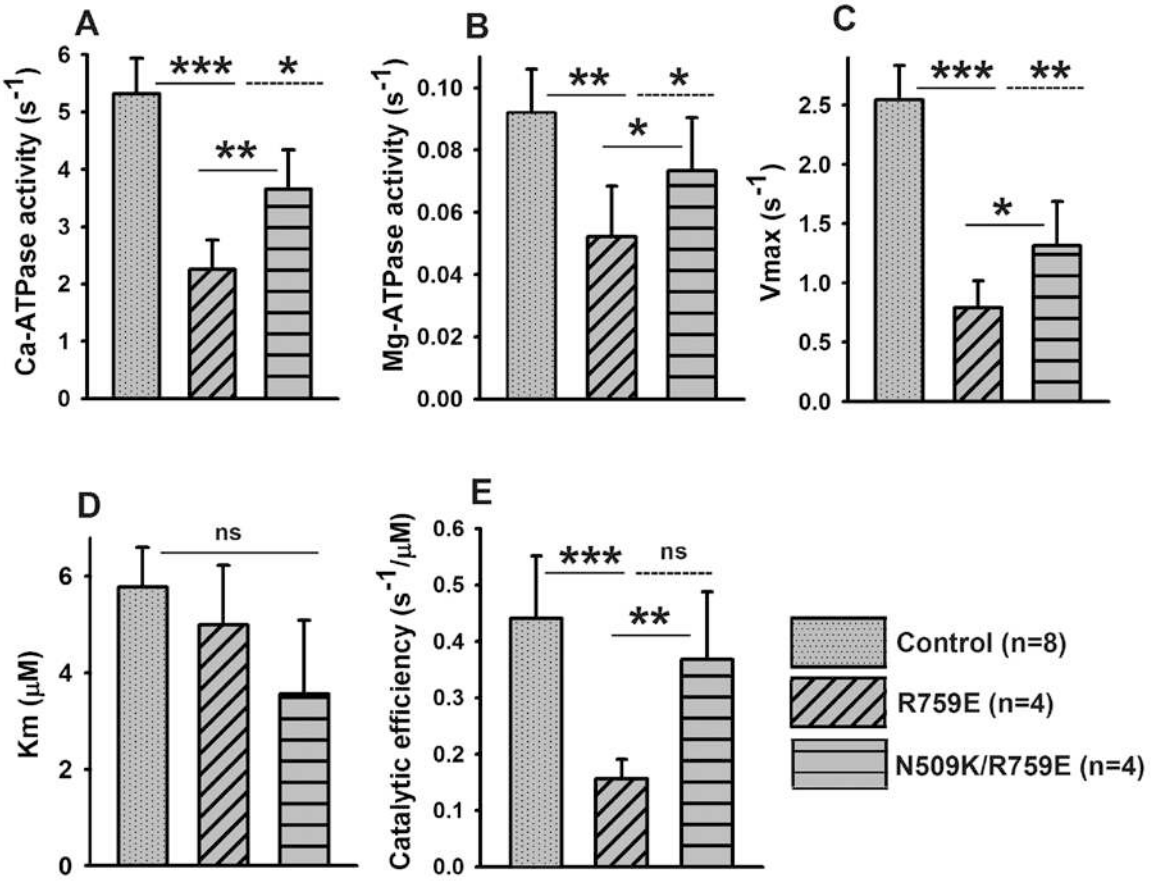
A
B
C
D
E
Ca-ATPase activity (s-1)
Mg-ATPase activity (s-1)
Vmax (s-1)
Km (μM)
Catalytic efficiency (s-1/μM)
***
**
*
ns
Control (n=8)
R759E (n=4)
N509K/R759E (n=4)

Figure 3:

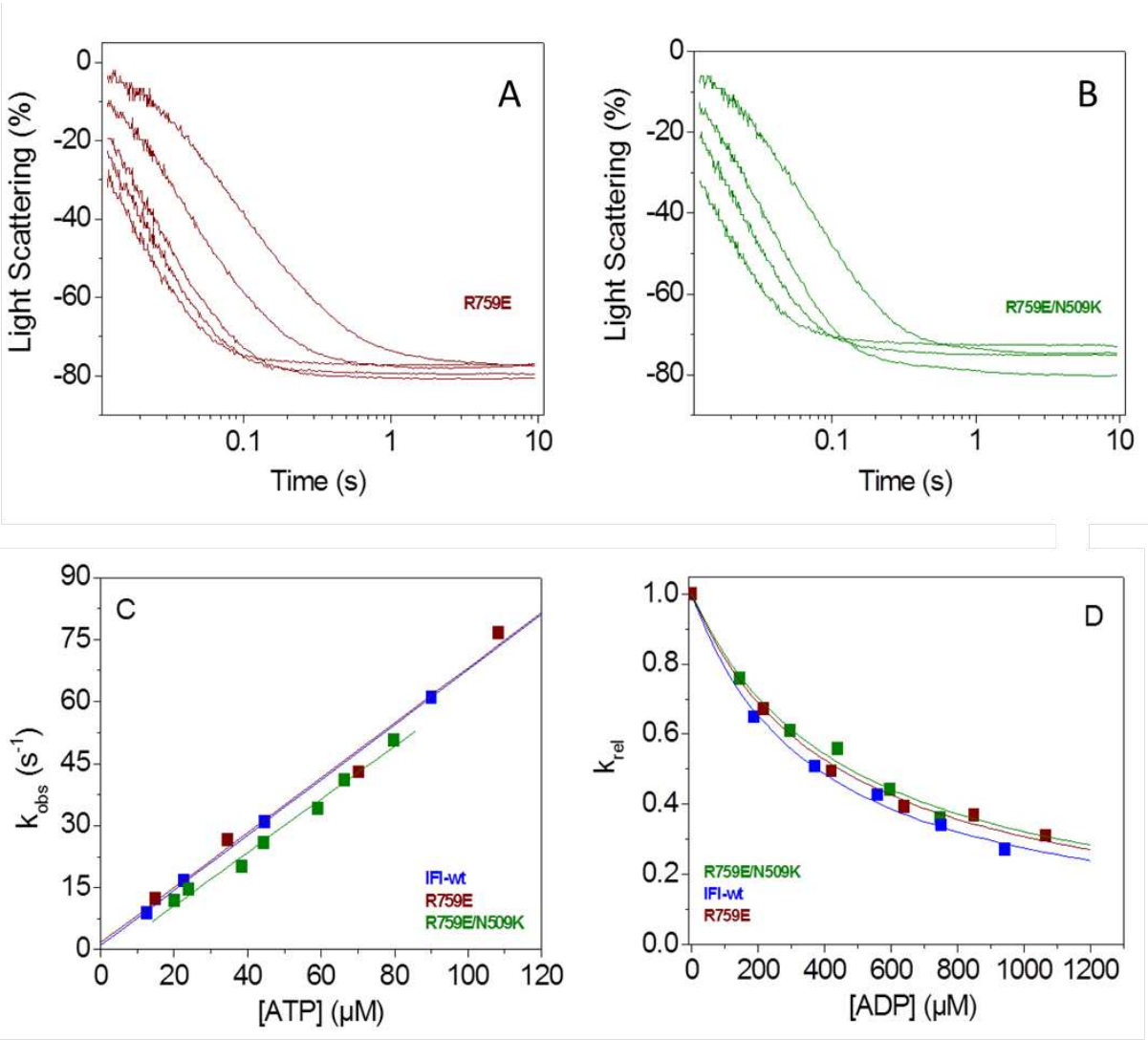
A
Light Scattering (%)
0
-20
-40
-60
-80
R759E
0.1
1
10
Time (s)
B
Light Scattering (%)
R759E/N509K
Time (s)
C
k_{obs} (s^{-1})
90
75
60
45
30
15
0
IFI-wt
R759E
R759E/N509K
0
20
40
60
80
100
120
[ATP] (μM)
D
k_{rel}
1.0
0.8
0.6
0.4
0.2
0.0
R759E/N509K
IFI-wt
R759E
0
200
400
600
800
1000
1200
[ADP] (μM)

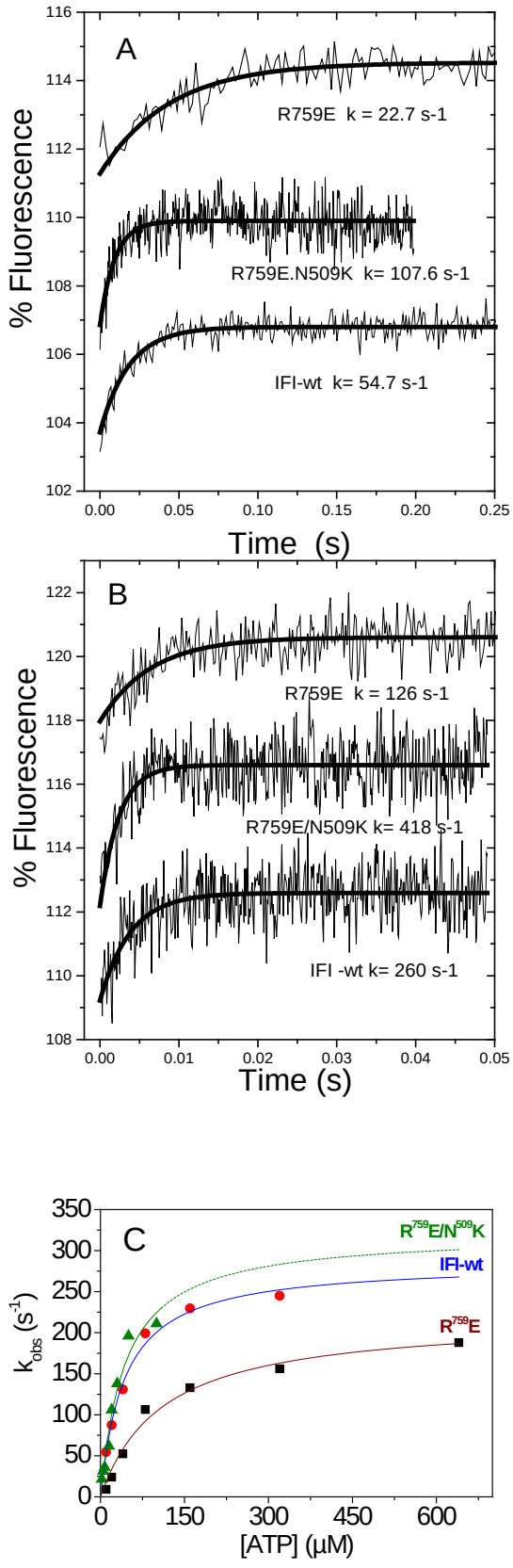
A
R759E k = 22.7 s-1
R759E.N509K k= 107.6 s-1
IFI-wt k= 54.7 s-1
% Fluorescence
Time (s)
B
R759E k = 126 s-1
R759E/N509K k= 418 s-1
IFI -wt k= 260 s-1
% Fluorescence
Time (s)
C
R759E/N509K
IFI-wt
R759E
kobs (s-1)
[ATP] (µM)

Figure 4

Figure 5:

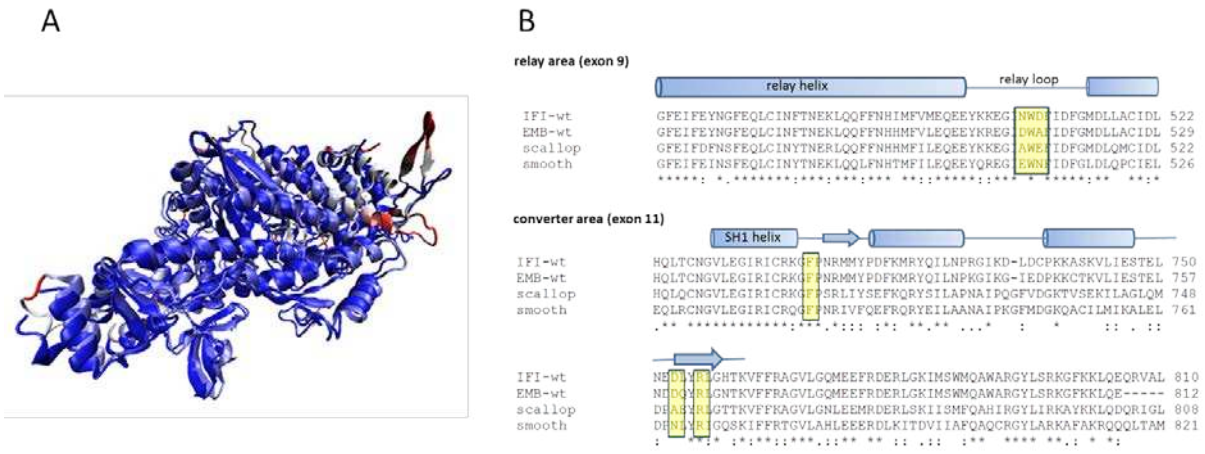
A
B
relay area (exon 9)
relay helix
relay loop
IFI-wt GFEIFEYNGFEQLCINFTNEKLQQFFNHIMFVMEQEEYKKEGINWDFIDFGMDLLACIDL 522
EMB-wt GFEIFEYNGFEQLCINFTNEKLQQFFNHHMFVLEQEEYKREGIDWAFIDFGMDLLACIDL 529
scallop GFEIFDFNSFEQLCINYTNERLQQFFNHHMFILEQEEYKKEGIAWEFIDFGMDLQMCIDL 522
smooth GFEIFEINSFEQLCINYTNEKLQQLFNHTMFILEQEEYQREGIEWNFIDFGLDLQPCIEL 526
converter area (exon 11)
SH1 helix
IFI-wt HQLTCNGVLEGIRICRKGFPNRMMYPDFKMRYQILNPRGIKD-LDCPKKASKVLIESTEL 750
EMB-wt HQLTCNGVLEGIRICRKGFPNRMMYPDFKMRYQILNPKGIKG-IEDPKKCTKVLIESTEL 757
scallop HQLQCNGVLEGIRICRKGFPSRLIYSEFKQRYSILAPNAIPQGFVDGKTVSEKILAGLQM 748
smooth EQLRCNGVLEGIRICRQGFPNRIVFQEFRQRYEILAANAIPKGFMDGKQACILMIKALEL 761
IFI-wt NEDLYRLGHTKVFFRAGVLGQMEEFRDERLGKIMSWMQAWARGYLSRKGFKKLQEQRVAL 810
EMB-wt NEDQYRLGNTKVFFRAGVLGQMEEFRDERLGKIMSWMQAWARGYLSRKGFKKLQE----- 812
scallop DEAEYRLGTTKVFFKAGVLGNLEEMRDERLSKIISMFQAHIRGYLIRKAYKKLQDQRIGL 808
smooth DENEYRIGQSKIFFRTGVLAHLEEERDLKITDVIIAFQAQCRGYLARKAFAKRQQQLTAM 821

Figure 6:

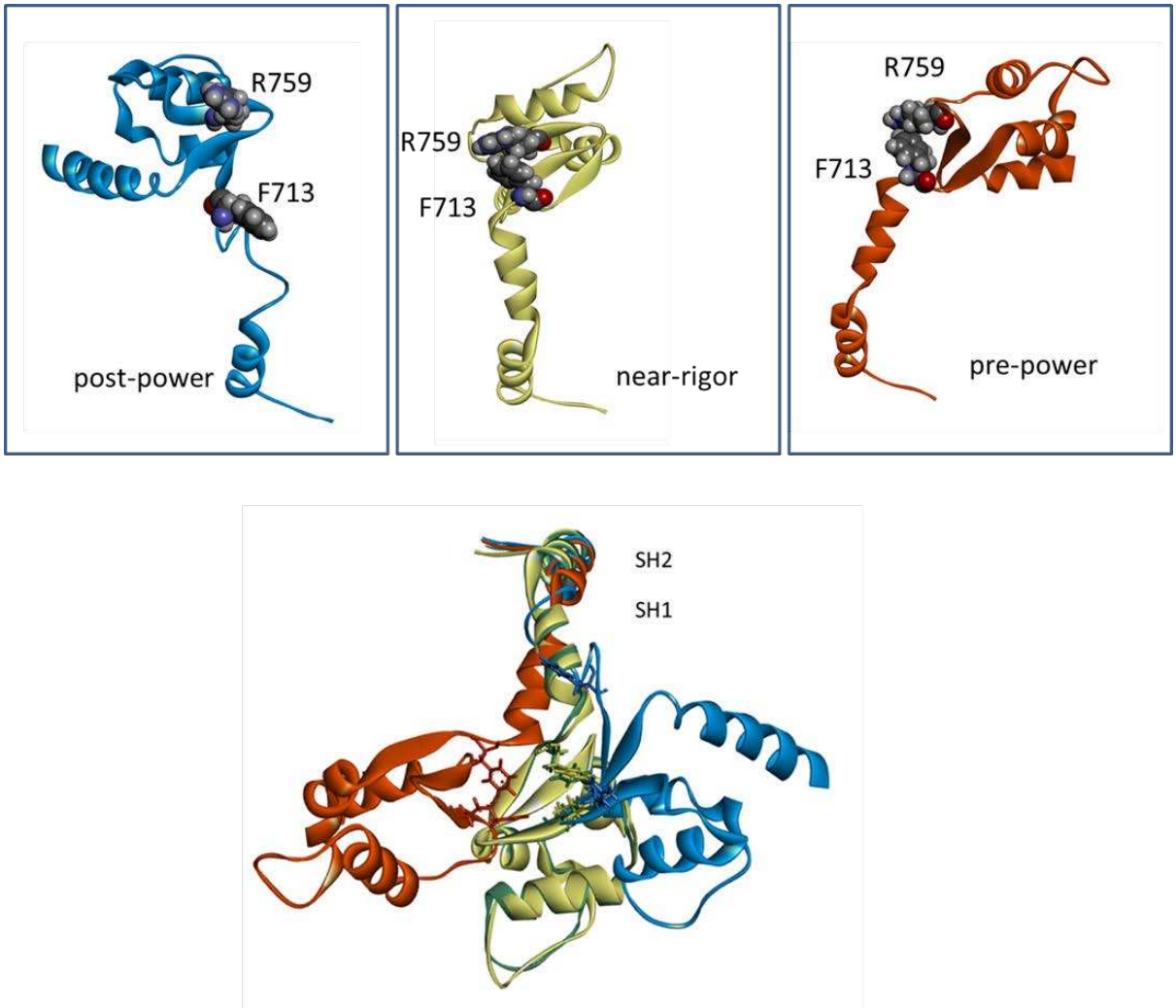
R759
F713
post-power
R759
F713
near-rigor
R759
F713
pre-power
SH2
SH1

Figure 7:

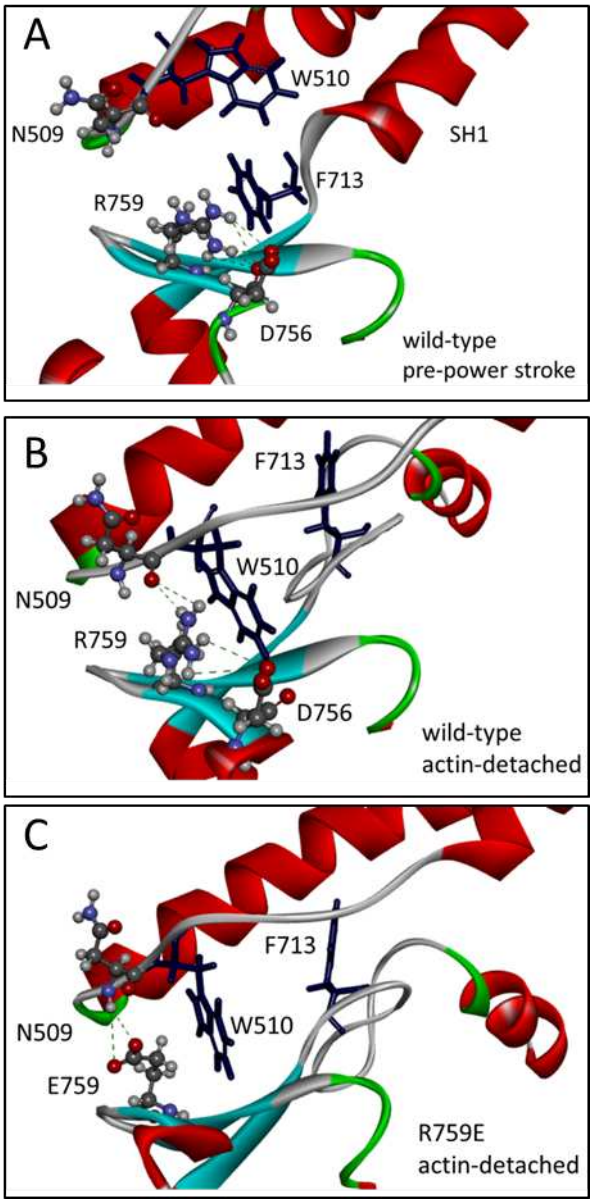
A
W510
N509
SH1
F713
R759
D756
wild-type
pre-power stroke
B
F713
W510
N509
R759
D756
wild-type
actin-detached
C
F713
N509
W510
E759
R759E
actin-detached

Figure 8:

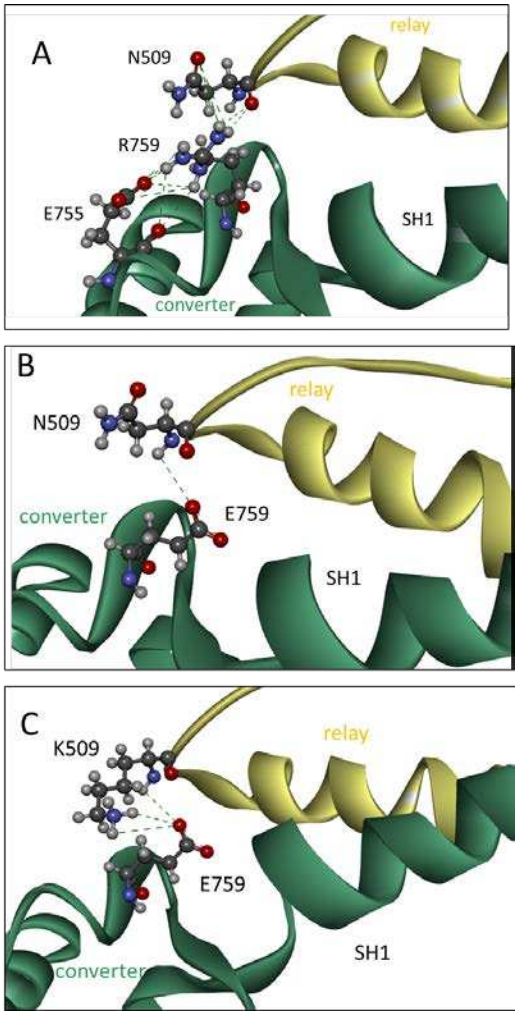
A
N509
relay
R759
E755
SH1
converter
B
N509
relay
converter
E759
SH1
C
K509
relay
E759
SH1
converter

Scheme 1:

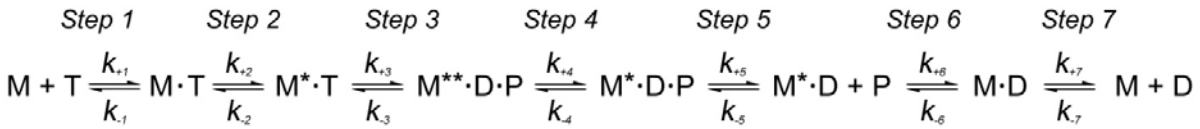

Scheme 2: